



Neural crest-derived mesenchymal progenitor cells enhance cranial allograft integration

Juliane D. Glaeser^{1,2,3,4} | Phillip Behrens^{1,3} | Tina Stefanovic^{1,2,3} |
 Khosrowdad Salehi^{1,2,3} | Angela Papalamprou^{1,2,3} | Wafa Tawackoli^{1,2,3,4,5,6} |
 Melodie F. Metzger^{3,7} | Samuel Eberlein^{3,4} | Trevor Nelson^{3,4} |
 Yasaman Arabi^{1,2,3} | Kevin Kim^{2,7} | Robert H. Baloh^{2,6} | Shiran Ben-David^{2,3,4} |
 Doron Cohn-Schwartz^{4,8} | Robert Ryu^{1,3} | Hyun W. Bae^{1,3} | Zulma Gazit^{2,3,4}  |
 Dmitriy Sheyn^{1,2,3,4,6} 

¹Orthopaedic Stem Cell Research Laboratory, Cedars-Sinai Medical Center, Los Angeles, California

²Board of Governors Regenerative Medicine Institute, Cedars-Sinai Medical Center, Los Angeles, California

³Department of Orthopedics, Cedars-Sinai Medical Center, Los Angeles, California

⁴Department of Surgery, Cedars-Sinai Medical Center, Los Angeles, California

⁵Biomedical Imaging Research Institute, Cedars-Sinai Medical Center, Los Angeles, California

⁶Department of Biomedical Sciences, Cedars-Sinai Medical Center, Los Angeles, California

⁷Orthopaedic Biomechanics Laboratory, Cedars-Sinai Medical Center, Los Angeles, California

⁸Division of Internal Medicine, Rambam Health Care Campus, Haifa, Israel

Correspondence

Dmitriy Sheyn, PhD, Board of Governors Regenerative Medicine Institute, Department of Orthopedics, Department of Surgery, Department of Biomedical Sciences, Cedars-Sinai Medical Center, AHSP A8308, 8700 Beverly Boulevard, Los Angeles, CA 90048. Email: dmitriy.sheyn@csmc.edu

Funding information

NIH/NIAMS, Grant/Award Number: K01AR071512; Musculoskeletal Transplant Foundation for Young investigator award

Abstract

Replacement of lost cranial bone (partly mesodermal and partly neural crest-derived) is challenging and includes the use of nonviable allografts. To revitalize allografts, bone marrow-derived mesenchymal stromal cells (mesoderm-derived BM-MSCs) have been used with limited success. We hypothesize that coating of allografts with induced neural crest cell-mesenchymal progenitor cells (iNCC-MPCs) improves implant-to-bone integration in mouse cranial defects. Human induced pluripotent stem cells were reprogramed from dermal fibroblasts, differentiated to iNCCs and then to iNCC-MPCs. BM-MSCs were used as reference. Cells were labeled with luciferase (Luc2) and characterized for MSC consensus markers expression, differentiation, and risk of cellular transformation. A calvarial defect was created in non-obese diabetic/severe combined immunodeficiency (NOD/SCID) mice and allografts were implanted, with or without cell coating. Bioluminescence imaging (BLI), micro-computed tomography (μ CT), histology, immunofluorescence, and biomechanical tests were performed. Characterization of iNCC-MPC-Luc2 vs BM-MSC-Luc2 showed no difference in MSC markers expression and differentiation in vitro. In vivo, BLI indicated survival of both cell types for at least 8 weeks. At week 8, μ CT analysis showed enhanced structural parameters in the iNCC-MPC-Luc2 group and increased bone volume in the BM-MSC-Luc2 group compared to controls. Histology demonstrated improved integration of iNCC-MPC-Luc2 allografts compared to BM-MSC-Luc2 group and controls. Human osteocalcin and collagen type 1 were detected at the allograft-host interphase in cell-seeded groups. The iNCC-MPC-Luc2 group also demonstrated improved biomechanical properties compared to BM-MSC-Luc2 implants and cell-free controls. Our results show an improved integration of iNCC-

MPC-Luc2-coated allografts compared to BM-MS-C-Luc2 and controls, suggesting the use of iNCC-MPCs as potential cell source for cranial bone repair.

KEYWORDS

allograft, bone healing, cranial repair, MSC, neural crest cells

1 | INTRODUCTION

Cranial bone loss due to trauma, decompressive craniotomy, or tumor resection continues to present a major clinical challenge.¹ Spontaneous reossification occurs only rarely, even in infants.² Bone grafts are typically used to repair cranial defects. Approximately 1.6 million bone grafts are used in the United States each year to regenerate bone loss due to trauma or disease.³ Autologous bone grafting is considered the “gold standard” due to its ability to stimulate new bone formation.⁴ However, bone harvesting is not always possible, painful, and is associated with donor site morbidity.⁴ Other options involve bone grafts harvested from cadavers (ie, allografts). Ease of procurement and availability make the use of allografts attractive. However, since an allograft consists of a nonviable tissue, it can only function as an osteoconductive scaffold and cannot stimulate new bone formation. Hence, allograft healing is passive and occurs at an extremely slow rate, since it relies upon invasion of host cells and tissues.⁵⁻⁷ Osteoinductive agents, known to stimulate new bone formation, include recombinant growth factors, such as bone morphogenetic proteins (BMP)-2 and -7.^{8,9} Due to their high cost and limited applicability, these proteins are only used to treat small bone lesions. In addition, safety concerns have been raised about the use of these proteins.¹⁰ Without the help of osteoinductive agents, however, cranial allograft integration into the host bone is challenging, due to the limited reservoir of resident mesenchymal stromal cells (MSCs) in the membranous bones of craniofacial complex.¹¹ A recent clinical study reported the use of a graft cultured with MSCs for treating 13 cases of craniofacial defects.¹² Allogeneic MSCs on a ceramic carrier and polymer scaffold have also shown to produce viable bone and healing of a cranial void during cranial reconstruction.¹ A combination of allografts and MSCs has produced positive results in rodent long bone defects.^{13,14} In calvarial defects, treatment with allografts seeded with adipose tissue-derived osteoblastic cells alone or in combination with endothelial cells did not support bone formation.¹⁵ MSCs have been isolated from various adult tissues, including bone marrow, and are currently the most established cells for skeletal regeneration.¹⁶⁻¹⁸ However, their availability and self-renewal is limited. Furthermore, in a variety of organs the regenerative potential of MSCs appears to decline with aging.¹⁹⁻²¹ Therefore, a need for a potent and ideally inexhaustible source of MSCs to treat craniofacial defects is needed to regenerate cranial defects.

Major parts of the cranial skeleton and its stem cells originate from neural crest cells (NCCs), including the frontal and interparietal parts and the sagittal suture.^{22,23} Since healing cascades

Significance statement

Cranial bone loss presents a major clinical challenge. To replace lost bone in the cranium, autografts and allografts are being used. While autografts are limited, allografts lack osteoinductive cells and signals. This project addresses the ongoing demand on improving graft integration into critical-size cranial defects. This study evaluates the capability of induced neural crest cell-mesenchymal progenitor cells (iNCC-MPCs), derived from induced pluripotent stem cells, to revitalize decellularized allografts and to enhance allograft integration. Due to the neural crest origin of larger cranial bone sections, this cell type holds great promise for improving of cranial bone replacement.

have been shown to recapitulate processes that occur during bone development, NCC-derived mesenchymal progenitor cells (MPCs) may be beneficial as cell therapeutic option compared to bone marrow-derived (BM)-MSCs that are usually isolated from iliac crest or long bones and originate in the mesoderm.²⁴ However, NCCs are rare in adults and ethical issues are associated with their isolation from embryonic tissues.²⁵ Therefore, most NCC studies have been performed in model organisms.^{25,26} To overcome the cell scarcity in adults and ethical concerns, NCCs can be derived from induced pluripotent stem cells (iPSCs).^{25,27-30} The discovery of iPSCs provides an inexhaustible source of patient-specific autologous cells that can be reprogrammed to NCCs and subsequently to MPCs.

In this study, we hypothesize that seeding allografts with iPSC-derived induced neural crest cell (iNCC)-MPCs will promote the integration of cranial allografts in mouse calvarial defects. To achieve this, iPSCs were differentiated into iNCCs and then into MPCs. Both cell types were characterized in terms of their marker expression and cell function *in vitro*. For *in vivo* testing, a critical size defect was created in mouse calvaria. The defect was filled with decellularized allografts with or without cell seeding. For cell seeding onto the allografts, either luciferase-transfected iNCC-MPCs or luciferase-transfected BM-MS-Cs were used. Allografts with no cell seeding were included as control. To evaluate cell viability and allograft integration, bioluminescence imaging (BLI), microcomputed tomography (μ CT) analysis,

biomechanical push-out tests, H&E, and immunofluorescence staining were performed.

2 | METHODS

2.1 | Experimental design

Mouse critical size calvarial defect repair using decellularized allografts with and without human stem cell coating was investigated. Cell types included were BM-MSCs and iNCC-MPCs. iNCC-MPCs were generated from iPSC-derived iNCCs using a previously described protocol.³⁰ BM-MSCs were obtained from human bone marrow aspirate (Lonza). Cells were transduced with a Lentiviral vector encoding for Luciferase2 (Luc2) reporter gene to allow for in vivo tracking, as previously reported³¹⁻³⁴ and characterized for their marker expression, differentiation potential, and risk of cellular transformation. For in vivo evaluation, a 5-mm round calvarial critical size defect was created in immunocompromised non-obese diabetic/severe combined immunodeficiency (NOD/SCID) mice (NOD.CB17-Prkdcscid/NCrHsd, Envigo) as previously reported^{35,36} and the following three experimental groups were implanted in a randomized fashion: (a) decellularized allografts only, (b) decellularized allografts seeded with BM-MSC-Luc2, and (c) decellularized allografts seeded with iNCC-MPC-Luc2. Animals were monitored for a duration of 8 weeks postsurgery: BLI was performed to monitor cell viability at the defect site and μ CT was done to evaluate the quantity and quality of new bone formation. After 8 weeks, animals were sacrificed and biomechanical testing, as well as histological and immunofluorescent stains was performed to further determine the implant integration of the different experimental groups (Graphical abstract).

Our study comprised a total of 42 NOD/SCID mice. With originally 67 NOD/SCID mice undergoing surgery, a total of 25 animals were not included in the study analysis due to the following reasons: (a) mice that died from unexpected anticipated outcomes, such as extensive bleeding during surgery ($n = 3$), or animals that did not recover from anesthesia (at surgery, BLI or CT; $n = 11$); (b) mice displaying implant shifting for more than 10% of the original position ($n = 11$). Animal exclusion resulted in the following final number of animals per group: (a) decellularized allografts only ($n = 15$), (b) BM-MSC-Luc2-seeded decellularized allografts ($n = 12$), and (c) iNCC-MPC-Luc2-seeded decellularized allografts ($n = 15$).

2.2 | Derivation of iNCC-MPCs and BM-MSCs, and labeling with Luc2

NCCs were differentiated from iPSCs, as previously published.³⁰ Briefly, human iPSCs, derived from dermal fibroblasts as previously reported,^{37,38} were differentiated into neural crest stem cells via incubation in defined conditions containing a cocktail of growth factors and two small-molecule compounds to activate Wnt signaling (BIO) and inhibit the Activin A/Nodal pathway (SB431542) for 11 to

14 days.²⁸ The neural crest culture media consisted of DMEM/F-12, 2% fetal bovine serum (FBS), 1xNEAA, 50 U/mL penicillin, 50 μ g/mL streptomycin, 50 μ g/mL ascorbic acid, 10 μ g/mL transferrin, 0.1 mM 2-mercaptoethanol, 1X trace elements A,B,C, 10 ng/mL heregulin β -1, 10 ng/mL activin A, 200 ng/mL insulin like growth factor-1, and 8 ng/mL fibroblast growth factor 2. Cell samples from various passages were fixed in 4% paraformaldehyde and processed for immunocytochemistry using antibodies against neurotrophin receptor (p75) and human natural killer-1 cell marker (HNK1) (for antibodies information, see Table S1). Flow cytometry was run on iNCCs with antibodies for p75 and HNK1, using an LSRFortessa cell analyzer (BD Biosciences) and FlowJo data analysis software.

Further differentiation of iNCCs to MPCs was performed by culturing the cells in standard Dulbecco's Modified Eagle Medium (DMEM) media (10% FBS) and passing them every 4 to 5 days as previously described.²⁸ Human BM-MSCs were isolated from whole bone marrow aspirate (Lonza), using standard method and plastic adherence, as previously described.³⁹⁻⁴² BM-MSCs and iNCC-MPCs were transduced with a lentiviral vector harboring the reporter gene luciferase2 (Luc2) under the constitutive ubiquitin promoter to allow in vivo imaging of cell survival, as previously reported.^{33,34}

2.3 | Cell characterization for mesenchymal properties

Both types of Luc2-transfected cell types were characterized for expression of consensus MSC markers (CD90, CD44, CD29, and CD105) using flow cytometry, as reported.^{43,44} At a confluence of 70%, the cells were detached using trypsin-EDTA, washed with phosphate-buffered saline (PBS), and resuspended in FACS buffer consisting of 2% albumin from bovine serum and 0.1% sodium azide in PBS. The cells were stained with mouse anti-human CD90-FITC (BD Biosciences Pharmingen, San Diego, California), mouse anti-human CD29-PB (EXBIO, Vetec, Czech Republic), and anti-human CD105-PE (AnCELL Corp., Stillwater, Minnesota); CD44-APC (559 942; BD Pharmingen, San Diego, California), and unspecific staining was normalized using the following isotypes: mouse IgG2a-FITC (Miltenyi Biotec, San Diego, California), mouse IgG1-PB (AbD Serotec, Raleigh, North Carolina), and mouse IgG1-PE (BD Biosciences Pharmingen), mouse IgG2b-APC (BD Biosciences Pharmingen), respectively. Cells were analyzed for expression of the antigens using an LSR Fortessa cell analyzer (BD, Heidelberg, Germany) and BD Diva software version 6.1.3 for data collection. Gating was done to include all live cells. Non-specific fluorescence was detected using isotypes alone and subtracted from the experiment's detection values. The iNCC-MPCs differentiation potential was confirmed by the cells' differentiation into the osteogenic and adipogenic lineages in vitro. Therefore, an alkaline phosphatase (ALP) assay and an Oil Red O staining⁴⁵ were performed after culturing of BM-MSCs and iNCC-MPCs in osteogenic media for 14 days and adipogenic media for 5 weeks, respectively. ALP values were normalized to the total protein content, which was determined via bicinchoninic acid assay. The risk of cellular

transformation of the iNCC-MPCs vs BM-MSCs was tested using a soft agar assay,⁴³ performed at weeks 1, 2, and 3 after seeding, according to manufacturer's protocol (Cytoselect, Cell Biolabs).⁴⁶ In addition, 1 million iNCC-MPCs or BM-MSCs were injected intramuscularly into immunocompromised NOD/SCID mice ($n = 5$). The mice were followed up weekly for 6 months for tumor or teratoma formation.

2.4 | Preparation of allografts

Structural allografts were harvested from fresh 67 C57BL/6J mouse cadavers using a trephine with inner diameter of 5 mm. Tissue harvest was performed in accordance to the approved IACUC protocol #007961. The allografts were scraped to remove any soft tissue and washed with PBS. For complete decellularization, the allografts were washed for 1 hour in PBS 0.1 wt%/vol% EDTA at room temperature (RT) with rotation, then incubated in the following solutions according to published protocols^{47,48}: first: in PBS 0.1 wt%/vol% EDTA and 10 mM Tris overnight at 4°C with rotation; second: PBS 10 mM Tris and 0.5 wt%/vol% sodium dodecyl sulfate for 24 hours at RT; third: enzymatic treatment with PBS 10 mM Tris, 50 U/mL DNase, 1 U/mL RNase for 5 hours at RT with rotation and sterilized with 70% EtOH overnight. Prior to changing the solutions, the allografts were washed for 1 hour with PBS at RT. Grafts were frozen at -80°C prior to implantation and were thawed 24 hours before the surgical procedure by placing them in serum free medium overnight. For cell coating, 2×10^5 BM-MSC-Luc2 or iNCC-MPC-Luc2 were resuspended in 12.5 μ L fibrin gel (Tisseel kit, Baxter). The fibrin-cell mixture was rapidly added onto the top of the allograft, which was incubated for at least 30 minutes at 37°C prior to implantation to allow gelation and attachment to the graft.

2.5 | Calvarial defect repair

Animal surgeries were performed in accordance to the approved IACUC protocol #007961 "Bone regeneration using stem cells in a mouse model," as previously reported.^{35,36} To create calvarial defects, the 8-week-old NOD/SCID mice were anesthetized by an intraperitoneal (IP) injection of ketamine/dexmedetomidine (75 mg/1 mg/kg, IP injection). Buprenorphine (0.05 mg/kg) was subcutaneously (SQ) injected for pain control. Animals were given thermal support for the duration of the anesthetic episode. The surgical site was aseptically prepped by thoroughly disinfecting with betadine or chlorhexidine. A straight sagittal incision (7 mm) was made over the calvaria and a circular full-thickness defect (a nonunion critical-size defect⁴⁹⁻⁵¹) was created at the lambdoid suture of the calvaria using a 5 mm outer-diameter trephine and removed with minimal penetration of the dura mater. This resulted in the removal of mesodermal parietal bone and neural crest derived interparietal bone. The allografts were placed in the calvarial defect, then fixed in position with 10 μ L fibrin gel (Tisseel kit, Baxter), after which the scalp was

sutured. Postsurgery, mice were given the anesthesia-reversing agent atipamezole (1 mg/kg body weight, IP injection) and a second dose of buprenorphine (0.05 mg/kg, SQ injection), which was repeated on day 1 postsurgery and afterward as needed. The antibiotic enrofloxacin was given twice daily for five consecutive days (5 mg/kg; 0.06 mL; SQ injection) to prevent infection. Mice were single housed for 2 weeks and then in pairs for the remaining duration of the study.

2.6 | Bioluminescence imaging

To measure the viability of the cells seeded on the grafts prior and postimplantation, Luc2 expression was quantified using in vivo BLI with IVIS Spectrum (PerkinElmer) at weeks 1, 2, 3, 4, 6, and 8, as described previously.^{33,34,52} BLI was performed in accordance to the approved IACUC protocol #06113. Mice were anesthetized using 2% isoflurane. An IP injection of 126 mg/kg body weight luciferin (Promega) in PBS was given 10 minutes before imaging. The image analysis was done using total influx data calculated from same size region of interest (ROI; 7 mm in diameter), normalized to the background noise of each image. BLI signals were normalized to signals detected on day 1 in each animal and plotted.

2.7 | Integration of calvarial allografts evaluated with μ CT

Bone formation was monitored by μ CT analysis in vivo, as previously described.^{36,53,54} The mice were scanned using a VivaCT 40 (SCANCO Medical AG, Switzerland) at the following time points: day 1, week 2, 4, and 8. Bone volume (BV), bone mineral density (BMD), and connectivity density (conn. dens.)⁵⁵ were included, as previously described.^{33,53} Briefly, microtomographic slices were acquired using an x-ray tube potential of 55 kVp and reconstructed at a spatial nominal resolution of 35 μ m. The defect margins were aligned to a standard position, and a cylindrical volume of interest (VOI) was defined (7 mm in diameter, including partial host bone in outer periphery, and average of 10-25 slices in depth). A constrained 3D Gaussian filter was used to partially suppress noise in the volumes. The bone tissue was segmented by using a global thresholding procedure. Week 2, 4, and 8 data were normalized to day 1 data obtained from the same animal to diminish variations.

2.8 | Biomechanical testing of calvarial defect repair

Biomechanical push-out tests were performed to evaluate the strength and stiffness of healing defects using methods similar to previous studies with modifications to accommodate the smaller dimensions of the mouse skull.⁵⁶⁻⁵⁸ Excessed skin and soft tissue was carefully removed from each calvarium. Afterward, specimens were

secured to the frame of a biaxial hydraulic testing machine (370.02 Bionix Testing System, MTS Systems Corp., Eden Prairie, Minnesota) with two custom 3D-printed plates, designed to match the mouse skull curvature. Calvaria were placed superior-side down on the bottom plate with the implant site centered over a 6 mm clearance hole (Figure 5A). The top plate was placed over the bottom plate and the two plates were screwed together after visually confirming alignment. A 4 mm diameter pin mounted to the actuator of the testing machine in line with a 1 kN load cell (661.18 Force Transducer, MTS Systems Corp.) was lowered onto the implant at a rate of 0.03 mm/s until a sizeable drop of load was detected. Load and displacement were continually recorded to generate a load-displacement curve. Maximum force was indicated as the highest load before failure and stiffness was determined as the slope of the linear region of the load-displacement curve. In addition to testing the experimental groups, age- and sex-matched naïve cranial samples ($n = 10$) were tested for comparison.

2.9 | Histological and immunofluorescent analyses

After sacrifice at week 8 postsurgery, the defect site including the allograft and surrounding bone tissue was explanted. Samples were fixed in 4% formaldehyde solution, decalcified by incubation in 0.5 M EDTA (pH 7.4), passed through a graded series of ethanol solutions, and embedded in paraffin. Five-micron-thick sections were cut from the paraffin blocks. H&E staining was performed to evaluate the morphological features of the healing process, graft-to-host osseointegration, and fibrous tissue formation as previously reported.^{54,59} For immunofluorescent staining, tissues were deparaffinized, and the antigens were retrieved by incubation in preheated Target Retrieval Solution (Dako, Carpinteria, California) overnight in 4°C. Nonspecific antigens were blocked by applying blocking serum-free solution (Dako). Slides were stained with primary antibodies, as detailed in Table S1. The primary antibodies were applied to the slides, after which the slides were incubated at 4°C overnight and washed using PBS; the slides were then incubated with secondary antibodies for 1 hour at room temperature. Finally, the slides were stained with 4',6-diamidino-2-phenylindole dihydrochloride (1 $\mu\text{g}/\text{mL}$) for 5 minutes in the dark. A VectaMount mounting medium (Vector Laboratories, Burlingame, California) was applied to the tissue. Images were captured using a Carl Zeiss Axio Imager Z1 fluorescent microscope (Carl Zeiss, Germany) equipped with ApoTome and AxioCam HRc cameras. Negative controls were processed using identical protocols while omitting the primary antibody to exclude nonspecific staining. Images were captured with 4 × 4 tile scans at ×20 objective.

2.10 | Statistical analysis

All statistical analyses were performed using Prism 7 or 8 (GraphPad, La Jolla, California); $P < .05$ was considered to be statistically significant. The outcome measurements were (a) MSC/MPC function, (b) BLI intensity, (c) μCT measures, and (d) biomechanical measures. Separately for

each dependent measure, two-way analysis of variance or mixed-effects analysis (BLI only) were performed using mean values with grouping of implant group; for multiple comparisons, appropriate post-hoc tests were used. In figures, median (min; max) values are shown.

3 | RESULTS

3.1 | iPSC-derived NCCs express neural crest markers and iNCC-MPCs show MSC characteristics

Following differentiation from iPSCs, iNCCs expressed both NGFR75 and HNK1 neural crest marker genes (Figure 1A,B). After further differentiation of iNCC to the mesenchymal progenitor phenotype, no differences in MSC surface marker expression (CD44, CD29, CD105, and CD73) was found in iNCC-MPC-Luc2 compared to BM-MSCLuc2 (Figure 1C). Following osteogenic differentiation for 14 days, a higher ALP activity was detected in both BM-MSCLuc2 and iNCC-MPC-Luc2 compared to day 0 ($P < .0001$). No differences in ALP activity between BM-MSCLuc2 and iNCC-MPC-Luc2 were detected (Figure 1D). Quantitative analysis of Oil-Red O stains showed an increase in lipid vacuoles in both BM-MSCLuc2 and iNCC-MPC-Luc2 in adipogenic vs maintenance medium at week 5 ($P < .0001$, Figure 1E). No differences in the Oil-Red O staining were found between BM-MSCLuc2 and iNCC-MPC-Luc2. The soft agar assay demonstrated a higher cell transformation rate in BM-MSCLuc2 vs iNCC-MPC-Luc2 at 1- and 4-weeks postseeding ($P < .05$, Figure 1F), but no statistical differences were detected at week 2. A teratoma formation assay in vivo did not result in tumor or teratoma formation in any animal injected with iNCC-MPC-Luc2 or BM-MSCLuc2, and the cells were not detected at the implantation site at 6 months post-injection. Sample size for Figure 1 data analysis was three per group.

3.2 | BM-MSCLuc2 and iNCC-MPC-Luc2 both survive on allografts after implantation

To verify survival of the cells on the allograft after implantation, BLI of Luc2-transfected cells was performed (Figure 2A). Both cell types were detectable for the period of evaluation (8 weeks) (Figure 2B,C). At week 1 postimplantation of the allografts, the average BLI value increased in both cell types. At week 2, a further increase in BLI signal was detected in the iNCC-MPC-Luc2 group, indicating cell proliferation at the site of implantation. This signal was reduced over time, but still detectable at week 8 in both groups (Figure 2B,C). Sample size for Figure 2 data analysis was nine per group.

3.3 | Improvement of bone quantity and quality at the host-implant interphase in cell-seeded allografts

Sagittal and coronal sections of reconstructed μCT 3D images obtained at day 0 and weeks 2, 4, and 8 postsurgery showed new

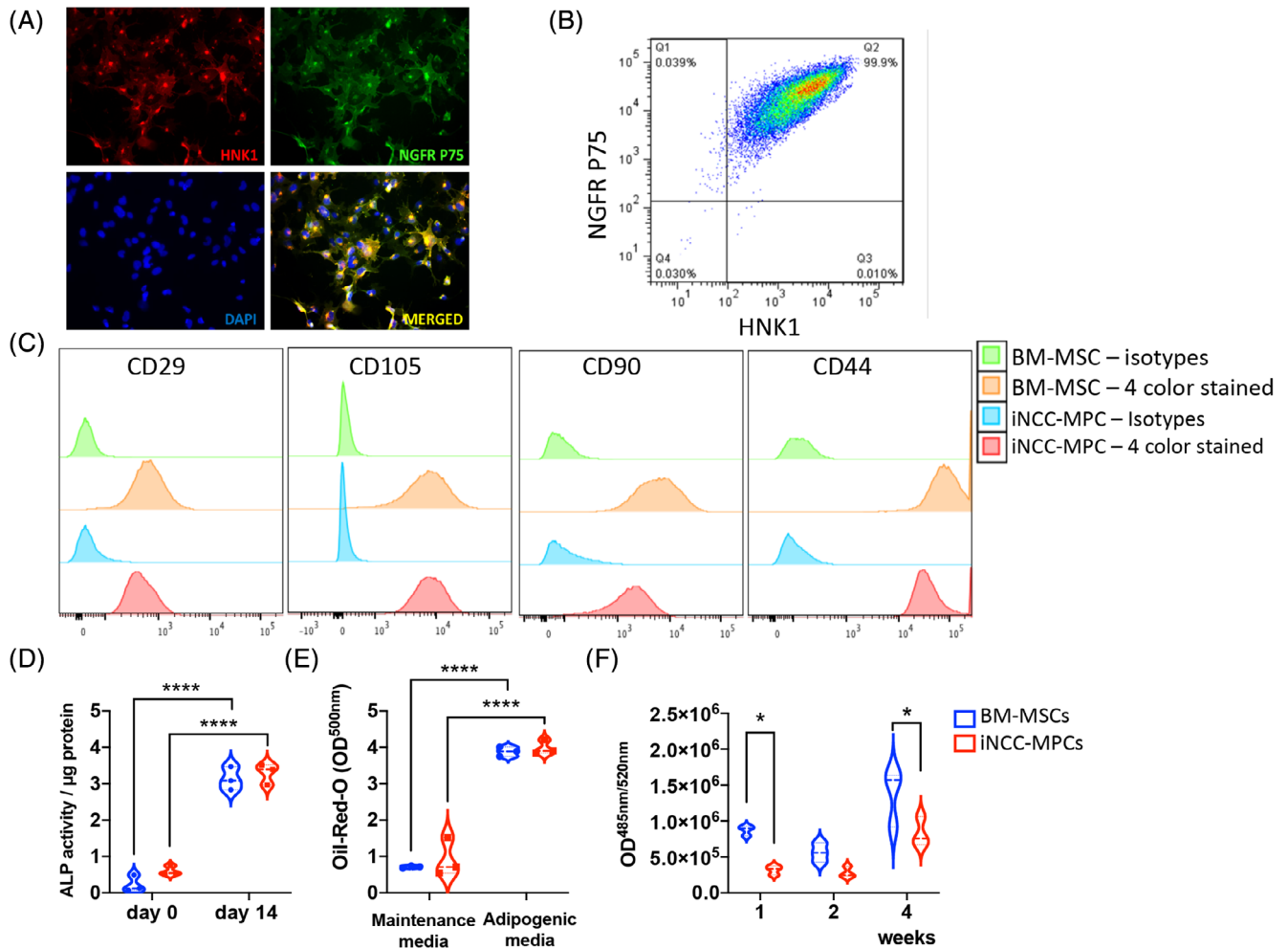


FIGURE 1 iNCC-MPCs and BM-MSCs show no differences in MSC consensus marker expression and cell differentiation in vitro. A, Immunofluorescence images and, B, flow cytometry data of iNCCs stained with the neural crest markers NGFR P75 and HNK1 are shown. C, Flow cytometry data showing MSC consensus marker expression in iNCC-MPC-Luc2 compared to BM-MSC-Luc2. D, ALP activity assay and, E, Oil-Red O assay in BM-MSC-Luc2 and iNCC-MPC-Luc2 are displayed. F, Results of the soft agar assay are shown. * $P < .05$; **** $P < .0001$. $n = 3$. ALP, alkaline phosphatase; BM-MSCs, bone marrow-derived mesenchymal stromal cells; iNCC-MPCs, induced neural crest cell-mesenchymal progenitor cells

bone formation at the implant-host interphase in the BM-MSC-Luc2 and iNCC-MPC-Luc2 group groups during the course of the experiment (Figure 3A).

At week 8, the BM-MSC-Luc2-seeded allograft group showed increased BV compared to allograft only ($P < .05$) and iNCC-MPC-Luc2-seeded allograft groups ($P < .05$), all normalized to the volume of the graft and host junction at time of implantation (Figure 3B).

Connectivity density was increased in the iNCC-MPC-Luc2 group compared to control at weeks 2 ($P < .05$) and 4 ($P < .05$) and tended to be increased at week 8 ($P = .05$). Furthermore, higher connectivity density values were detected in iNCC-MPC-Luc2 compared to BM-MSC-Luc2 ($P < .01$, Figure 3C). Relative BMD was increased in the iNCC-MPC-Luc2 group compared to BM-MSC-Luc2 at weeks 4 ($P < .01$) and 8 ($P < .001$, Figure 3D). Sample size for Figure 3 data analysis was 10 for the BM-MSC group, 8 for the iNCC-MPC group, and 5 for the control group.

3.4 | Improved integration of iNCC-MPC-Luc2 seeded allografts

Histological analysis of the implantation side showed partial bone bridging in the experimental group containing iNCC-MPC-Luc2, characterized by new bone formation that combined allograft and host bone (Figure 4A). In contrast, no solid bone bridges were detected in the BM-MSCs-seeded allografts and in the control group. In the control group, large areas of fibrotic tissue were detected between allograft and host bone. In the BM-MSC group, the fibrotic tissue areas were smaller compared to the control group.

Immunofluorescent staining of the host-allograft junction (Figure 4B) showed cells expressing Luc2 reporter gene, indicating survival of the implanted cells for at least 8 weeks. Colocalization of Luc-expressing cells and human osteogenic marker expression (osteocalcin and collagen type 1) in the

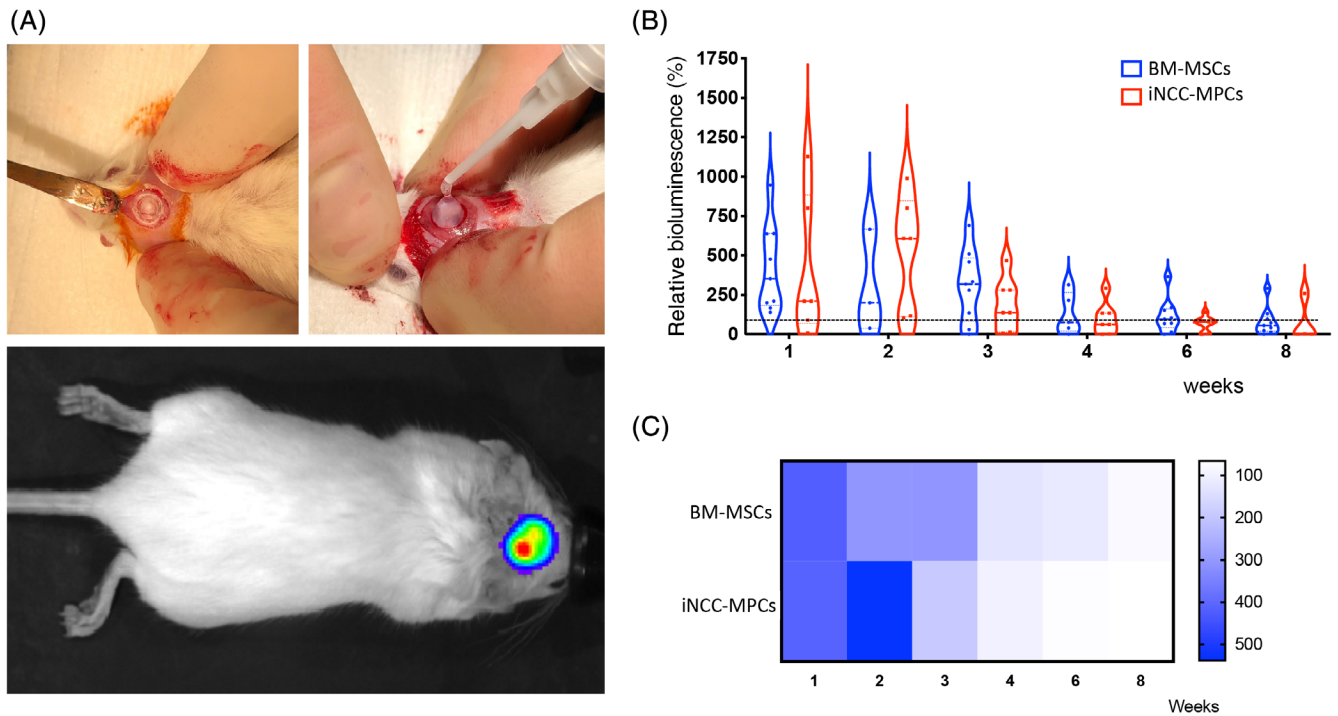


FIGURE 2 BM-MSC-Luc2 and iNCC-MPC-Luc2 are viable in vivo for at least 8 weeks. A, Top: BM-MSC-Luc2 and iNCC-MPC-Luc2 coated allografts were implanted and glued to the host bone with fibrin. Bottom: example of a BLI imaged mouse after implantation with Luc2-positive cell allografts. Mice were injected with Luciferin prior to undergoing an IVIS (Perkin Elmer) scanning. B, Relative bioluminescence in the different experimental groups normalized to signals recorded on day 1 in each animal (dotted line). C, A heat map comparing average BLI signals between BM-MSC-Luc2 and iNCC-MPC-Luc2 coated allografts. $n = 9$. BLI, bioluminescence imaging; BM-MSCs, bone marrow-derived mesenchymal stromal cells; iNCC-MPCs, induced neural crest cell-mesenchymal progenitor cells

interphase between the host calvarial bone and the allograft indicates differentiation of the cells into osteoblasts. No cells were identified to penetrate the allograft. Sample size for Figure 4 data analysis was three per group.

3.5 | Biomechanical properties are improved in calvarial defects treated with iNCC-MPC-Luc2-seeded allografts

Maximum force and stiffness of the different experimental groups was obtained at week 8 postsurgery (Figure 5A,B). The average maximum force recorded for nonsurgical naïve calvaria (23.4 ± 4.0 N) was significantly higher than calvaria implanted with either an uncoated control implant (16.4 ± 5.0 N) or BM-MSC coated implants (16.6 ± 6.3 N) ($P < .05$). The maximum force for calvaria implants coated with iNCC-MPCs (20.2 ± 6.4 N) was highest among the surgical implants groups and was not statistically different from naïve controls. The average calculated stiffness of iNCC-MPC-coated calvaria implants (67.3 ± 18.67 N/mm) was significantly greater than both allograft only (40.7 ± 14.2 N/mm) and BM-MSC-seeded implants (42.7 ± 8.5 N/mm) ($P < .01$), and had comparable stiffness to naïve nonsurgical controls (66.1 ± 12.5) (Figure 5C). Sample size for Figure 5 data analysis was 10 for the allograft, iNCC-MPCs, and intact bone groups, and 9 for the BM-MSC group.

4 | DISCUSSION

This is the first study to show that coating of decellularized allograft with iNCC-MPC-Luc2, MPCs differentiated from iPSC-derived NCCs, enhances allograft integration in a mouse critical-size calvarial defect compared to BM-MSC-Luc2-coated allograft or allograft only. Cells were successfully derived from the two cell sources, labeled with luciferase reporter gene and characterized in terms of their MSC marker expression and differentiation potential. A beneficial in vivo performance of iNCC-MPC-Luc2-seeded allografts in the treatment of cranial defects was demonstrated by an improved micro-architecture at the implant-host bone interphase, bone bridging, and improved biomechanical properties. In contrast, implantation of BM-MSC-Luc2-coated allografts resulted in increased levels of BV at the host-implant interphase at week 8 postsurgery, but did not result in an improved integration, and enhanced structural and biomechanical properties.

Characterization of the iPSC-derived NCCs demonstrated the cells to be 99.9% double positive for both HNK1 and p75 (NGFR). These data confirm the findings reported by Muhammad et al, showing a 99% double staining of p75 and HNK1 in the iPSC-derived NCCs in passage 9.³⁰ Further differentiation of the iNCCs into iNCC-MPCs was shown by the expression of the MSC consensus markers and their potential to differentiate into the osteogenic and adipose lineages.^{44,60} No significant differences in the differentiation potential

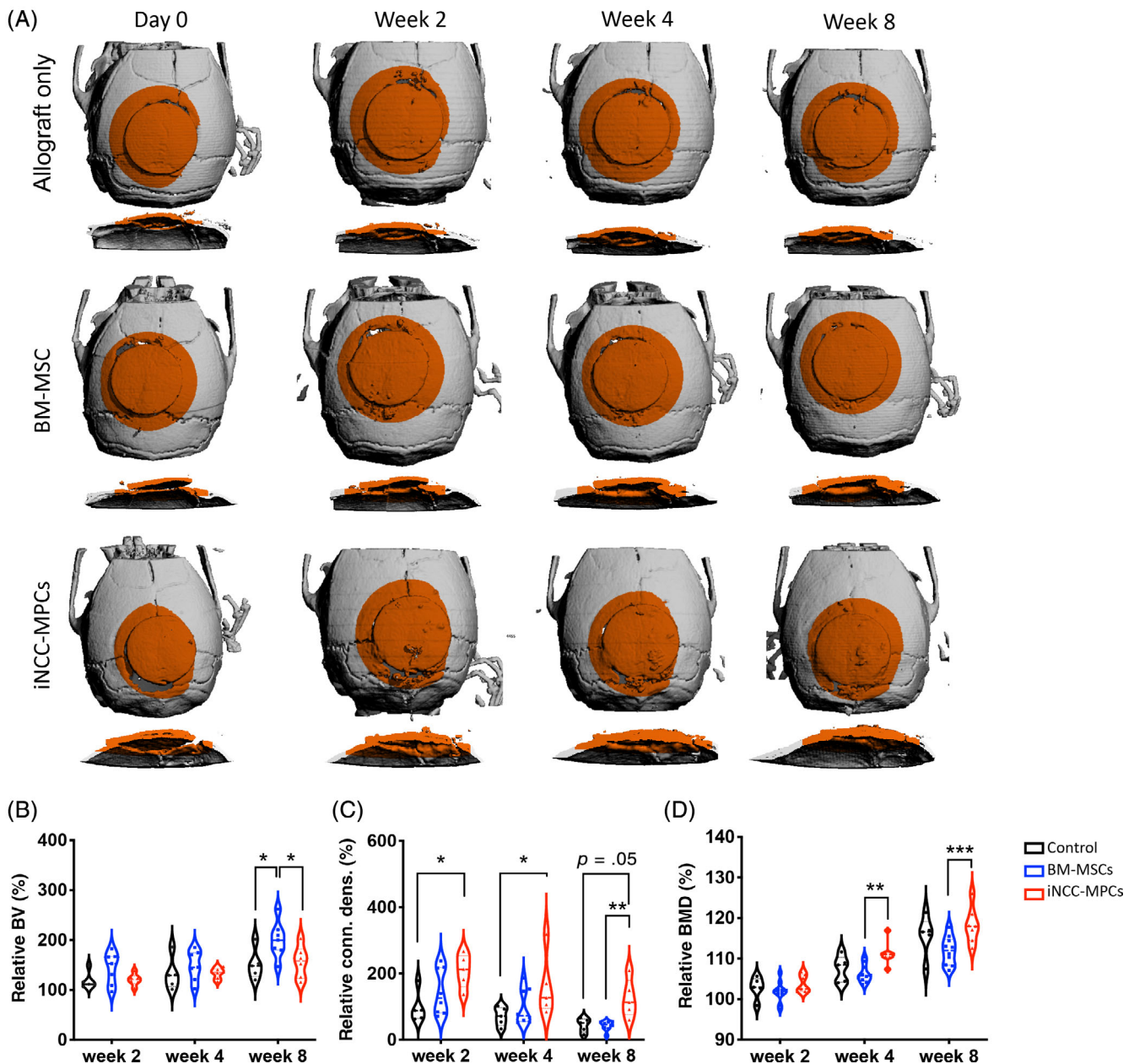


FIGURE 3 Bone volume is increased in defects treated with BM-MSC-seeded allografts, whereas connectivity density and BMD is improved in iNCC-MPC-seeded allografts. Shown are the results of the μ CT analysis of weeks 2, 4, and 8 relative to the day of the surgery. * $P < .05$; ** $P < .01$; *** $P < .001$. BM-MSC: $n = 10$, iNCC-MPC: $n = 8$, control: $n = 5$. μ CT, microcomputed tomography; BM-MSCs, bone marrow-derived mesenchymal stromal cells; BMD, bone mineral density; BV, bone volume; conn. dens., connectivity density; iNCC-MPCs, induced neural crest cell-mesenchymal progenitor cells

were detected between BM-MSC-Luc2 and iNCC-MPC-Luc2 cells. Interestingly, quantitative assessment of the cell transformation potential in vitro detected lower values in iNCC-MPC-Luc2 compared to BM-MSC-Luc2. The results of this preclinical technique⁶¹ indicate a low risk of malignancy of iNCC-MPCs compared to the clinically established BM-MSCs, a valuable information on the path to a potential clinical application of these cells.

Our results demonstrated the survival of allograft-seeded BM-MSC-Luc2 and iNCC-MPC-Luc2 cells for the study duration of 8 weeks. Other studies, in comparison, monitored the cell survival on

cranial bone grafts for a shorter duration.^{62,63} For example, a 4 week survival of adipose tissue-derived stem cells and BM-MSCs obtained from Col1a1^{GFP}; R26^{mTmG} mice seeded onto poly(lactic-co-glycolic acid) scaffolds and implanted into 2 mm calvarial defects was shown in vivo.⁶² In vitro, cell survival on a mineralized collagen bone scaffold for large-sized cranial bone defect repair in sheep was demonstrated, which was monitored for 7 days.⁶³

Our μ CT data demonstrate an improved BMD and connectivity density in the iNCC-MPC-Luc2 group, whereas higher BVs were achieved in the BM-MSC-Luc2 group at the 8-week time point at the

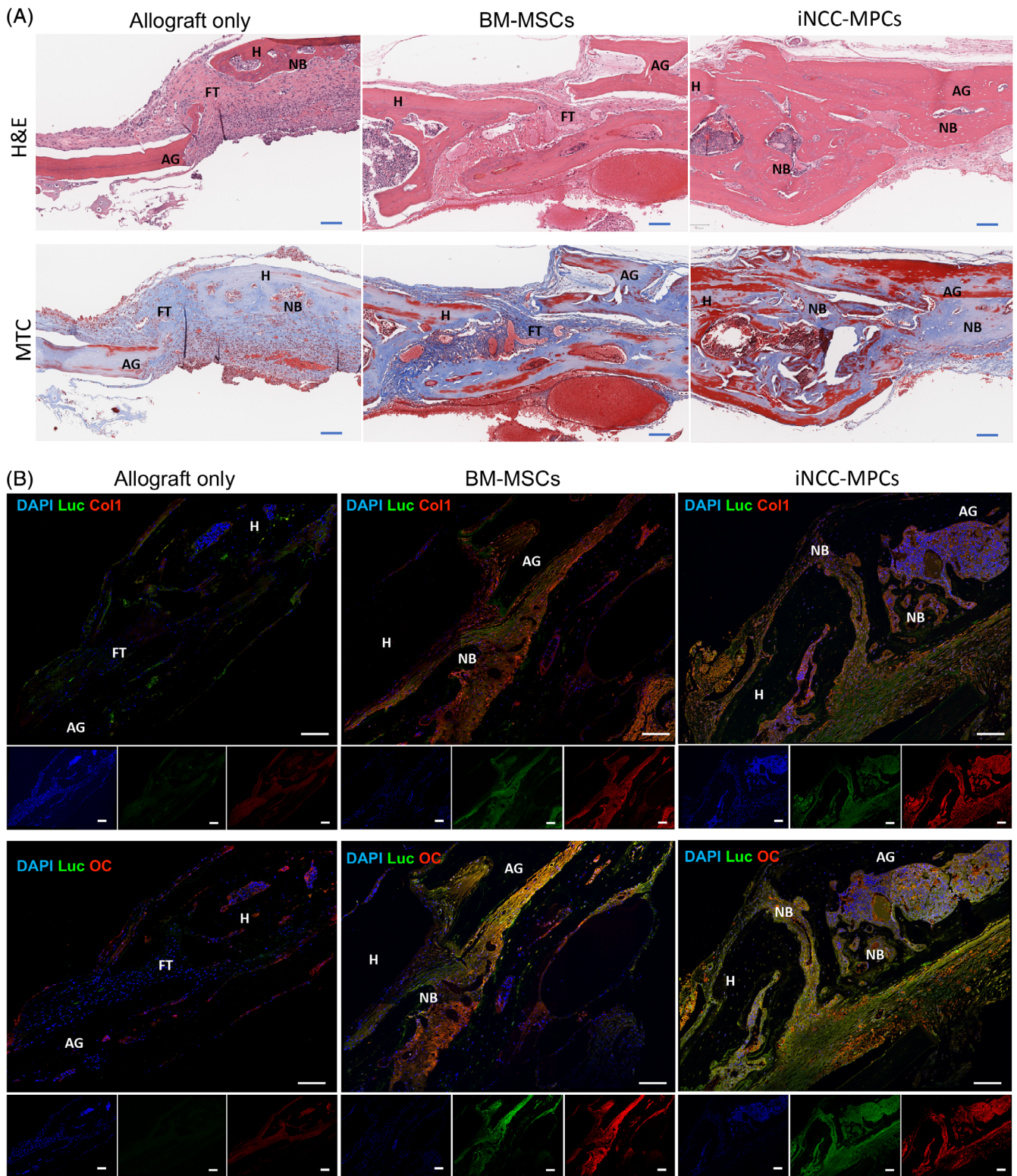


FIGURE 4 Partial bony bridging between allograft and host bone in the iNCC-MPC-Luc2 group. A, Cranial bones were harvested postsacrifice at week 8 postsurgery. Shown are representative H&E stained slides that resulted from sagittal cuts through the allografts. B, IF showing a DAPI, anti-Luc, and human osteocalcin or human collagen type 1 staining. AG, allograft; Col1, collagen type 1; FT, fibrotic tissue; HB, host bone; NB, new bone; OC, osteocalcin. Small images on the bottom show the single channels of each IF staining. Scale bars indicate 100 μ m in all images. $n = 3$. AG, allograft; Col1, collagen type 1; DAPI, 4',6-diamidino-2-phenylindole dihydrochloride; FT, fibrotic tissue; HB, host bone; IF, immunofluorescence; iNCC-MPCs, induced neural crest cell-mesenchymal progenitor cells; NB, new bone; OC, osteocalcin

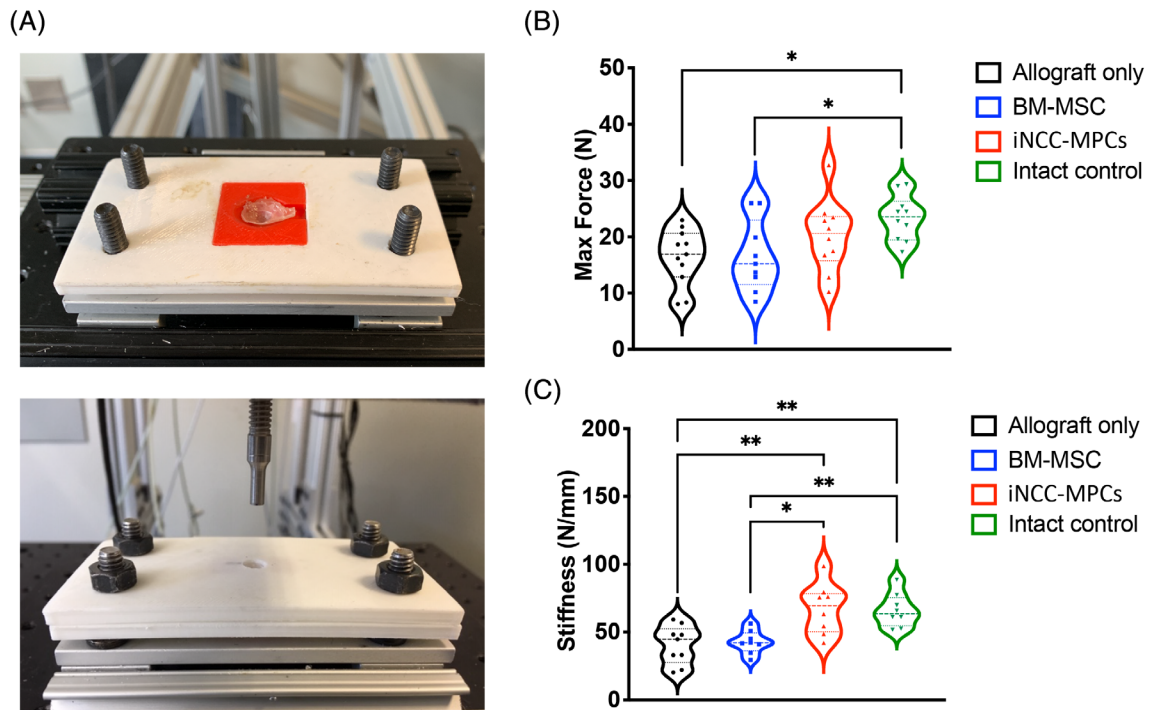


FIGURE 5 Biomechanical properties are improved in calvarial defects treated with -Luc2-seeded iNCC-MPC allografts. A, Top: A 3D printed bottom plate matching the curvature of the cranium was aligned to accommodate the pin of the biomechanical testing machine. Bottom: A 3D printed top plate was added and fixated with screws. Shown are (B) the maximum force and (C) the stiffness of the experimental groups and intact controls. * $P < .05$; ** $P < .01$. Allograft: $n = 10$, BM-MSC: $n = 9$, iNCC-MPC: $n = 10$, intact: $n = 10$. BM-MSCs, bone marrow-derived mesenchymal stromal cells; iNCC-MPCs, induced neural crest cell-mesenchymal progenitor cells

VOI (implant-host interphase). Similar to our study, an increase in BV in rat cranial defects in response to application of BM-MSCs combined with a collagen membrane was shown between 6 and 10 weeks.⁶⁴ In contrast, addition of MSCs to polyetherketoneketone scaffolds did not improve the BV at the defect site in calvarial sheep defects.⁶⁵ Differences may be due to the animal model, defect size, and performance of the carrier itself. To achieve solid bone fusion, other measures such as BMD and bone microarchitecture play an important role.⁶⁶ BMD has been shown to be a consistent predictor of bone strength for cortical bone in rat.⁶⁷ Furthermore, BMD values correlate with improvements in bone microarchitecture,⁶⁶ including connectivity density.⁶⁸ These findings indicate an enhanced bone quality in the iNCC-MPC-Luc2 group compared to the BM-MSC-Luc2 group.

To determine and compare functional load bearing between cranial implants, biomechanical push-out testing was performed. While calvaria are subjected to minimal biomechanical stresses during normal activities of daily living, it is important that regenerated calvarial bone can sufficiently withstand the large deforming forces that occur during a traumatic event to ensure the underlying neurological structures are adequately protected. In addition, the biomechanical testing data helps validate the qualitative and quantitative μ CT differences observed between groups. On average, iNCC-MPC-coated implants had greater strength and stiffness compared to both uncoated and BM-MSC coated cranial implants with values that were comparable to naïve cranial samples. This suggests the improved graft integration, as

demonstrated by increased BMD and connectivity density in iNCC-MPC seeded implants, translated to improved biomechanical properties and functional outcomes.

Histological evaluation of the implant-host bone interphase demonstrated partial bone bridging in the iNCC-MPC-Luc2 group, whereas only fibrotic bridges were observed in the BM-MSC-Luc2 and control groups at 8 weeks after surgery. While the iNCC-MPC-Luc2 group performed better than the other groups, the bone bridging success was still suboptimal. A possible explanation to that might be the lack of exogenous osteoinductive factors in this study. For example, BM-MSC-seeded BMP-6/nHAG/GMS scaffolds significantly accelerated new bone formation in an 8 mm calvarial defect in rat.⁶⁹ However, addition of osteogenic factors like bone morphogenetic proteins increases the complexity of the treatment and may cause additional difficulties on the path to clinical translation due to previously reported side effects associated with BMPs.⁷⁰

Differences between BM-MSC-Luc2 and iNCC-MPC-Luc2 groups in vivo, but not in vitro, might be due to similar cell intrinsic capacities but different cell responses to an in vivo environment comprising bone of mesodermal and neural crest origin. While BM-MSCs may respond to these signals by an increase in factors leading to a higher BV, iNCC-MPC-Luc2 may rather respond by an expression of factors that stimulate the bone's microarchitecture. Mechanisms that were postulated involve fibroblast growth factor (FGF), BMP, Wnt, and transforming growth factor beta (TGF- β) signaling, and were shown to

be differentially and even inversely activated in neural crest-derived and mesoderm-derived calvarial bone.²³

5 | SUMMARY AND CONCLUSION

In summary, this study demonstrates that seeding of decellularized allografts with MSCs derived from iNCCs enhances cranial allograft integration into host bone compared to allografts seeded with bone marrow-derived MSCs and allografts only. This was shown by an improved bone microarchitecture and by bone bridging at the interphase between host bone and allograft. The suggested mechanism involves stimulation of the iNCC-MPC-Luc2 cell function in the cranial bone environment because no difference in cell marker expression and cell function between BM-MSC-Luc2 and iNCC-MPC-Luc2 were detected *in vitro*. Evidence of cell viability along with an expression of human osteogenic markers indicates a direct contribution of the cells to the new bone formation. However, release of cell signals may also stimulate the host environment to form new bone.

Based on our results, iNCC-MPCs may be a potential candidate for repair of cranial defects, especially in the frontal bone, because it is neural crest-derived. While iNCC-MPCs may be more potent when placed in this environment, BM-MSCs may be more efficient in repairing distinct parietal defects. Indeed, successful rat calvarial defect regeneration in response to implantation of human BM-MSC spheroids into parietal bone was shown.⁷¹ However, this hypothesis should be evaluated in more detail in future studies. Furthermore, the mechanism of induction of new bone in response to the cell seeded allografts should be tested.

This study is not without limitations: about 40% of the animals receiving surgery could not be included. Seventeen percentage of the animals did not wake up from anesthesia, which occurred at different time points (surgery, BLI, or μ CT). In this study, the mice were anesthetized by an IP injection of ketamine/dexmedetomidine. Although we tested the dosing carefully prior to study start, several animals did not tolerate the anesthesia during the 8-week follow-up period. Five percentage of the animals died during the surgery from bleeding. Since the mouse cranium is very thin, bleeding can easily happen when drilling the skull. Seventeen percentage were excluded from the analysis due to implant shifting. Clinical grade fibrin glue was used for implant fixation, as it is known to be a nontoxic. However, it did not prevent graft shifting in several cases, as verified by μ CT 3D image reconstruction at day 0. Consequently, these animals were excluded from the study. Also, our study compared primary BM-MSC with induced iNCC-MPCs. While the significant difference in the ossification characteristics exhibited by those two cell types are likely due to differences in their developmental origin, it cannot be excluded that cell processing contributed to this effect. In future studies, iMSCs⁴³ from a matching donor should be used for comparison with iNCC-MPCs to draw more specific conclusions.

ACKNOWLEDGMENTS

This study was supported by the Musculoskeletal Transplant Foundation for Young investigator award to D.S. and by NIH/NIAMS K01AR071512 to D.S. The authors wish to acknowledge Cedars-Sinai

Imaging Core facility for performing the μ CT scans and Biobank and Translational Research Core for performing the histological analysis and scanning the slides.

CONFLICT OF INTEREST

M.F.M. declared research funding from Arthrex. R.H.B. declared consultant/advisory role with Mitochondria in Motion, Acurastem and Expert testimony for Irell. R.R. declared consultant/advisory role and stock ownership with OXOS Medical, Inc. All of the other authors declared no potential conflicts of interest.

AUTHOR CONTRIBUTIONS

J.D.G., W.T., M.F.M.: concept and design, collection and assembly of data, data analysis and interpretation, manuscript writing; P.B., T.S., K.S., S.E., T.N., Y.A.: collection and assembly of data, data analysis; A.P., S.B.-D., D.C.-S., R.R.: collection and assembly of data, data analysis and interpretation; K.K.: provision of study material, collection and assembly of data, data analysis; R.H.B.: provision of study material, data interpretation; H.W.B., Z.G.: concept and design, data interpretation; D.S.: concept and design, provision of study materials, collection and assembly of data, financial support, data analysis and interpretation, manuscript writing, final approval of manuscript.

DATA AVAILABILITY STATEMENT

The data that support the findings of this study are available from the corresponding author upon reasonable request.

ORCID

Zulma Gazit  <https://orcid.org/0000-0001-9176-0889>

Dmitriy Sheyn  <https://orcid.org/0000-0002-3333-1485>

REFERENCES

- Morrison DA, Kop AM, Nilasaroya A, Sturm M, Shaw K, Honeybul S. Cranial reconstruction using allogeneic mesenchymal stromal cells: a phase 1 first-in-human trial. *J Tissue Eng Regen Med*. 2018;12(2):341-348.
- Szpalski C, Barr J, Wetterau M, Saadeh PB, Warren SM. Cranial bone defects: current and future strategies [review] [in English]. *Neurosurg Focus*. 2010;29(6):E8.
- Regis J O'Keefe and Jeremy Mao. Bone tissue engineering and regeneration: from discovery to the clinic—an overview. *Tissue Eng Part B Rev*. 2011;17(6):389-392.
- Elsalanty ME, Genecov DG. Bone grafts in craniofacial surgery. *Craniofacial Trauma Reconstr*. 2009;2(3):125-134.
- Garbus DS, Masri BA, Czitrom AA. Biology of allografting [in English]. *Orthop Clin North Am*. 1998;29(2):199-204.
- Goldberg VM, Stevenson S. The biology of bone grafts. *Semin Arthroplasty*. 1993;4(2):58-63.
- Stevenson S. Biology of bone grafts [in English]. *Orthop Clin North Am*. 1999;30(4):543-552.
- Boden SD, Kang J, Sandhu H, Heller JG. Use of recombinant human bone morphogenetic protein-2 to achieve posterolateral lumbar spine fusion in humans: a prospective, randomized clinical pilot trial: 2002 Volvo Award in clinical studies. *Spine*. 2002;27(23):2662-2673.
- Einhorn TA. Clinical applications of recombinant human BMPs: early experience and future development. *J Bone Joint Surg Am*. 2003;85-A (suppl 3):82-88.

10. Carragee EJ, Hurwitz EL, Weiner BK. A critical review of recombinant human bone morphogenetic protein-2 trials in spinal surgery: emerging safety concerns and lessons learned. *Spine J.* 2011;11(6):471-491.
11. Zhao H, Feng J, Ho TV, Grimes W, Urata M, Chai Y. The suture provides a niche for mesenchymal stem cells of craniofacial bones. *Nat Cell Biol.* 2015;17(4):386-396.
12. Sandor GK, Numminen J, Wolff J, et al. Adipose stem cells used to reconstruct 13 cases with cranio-maxillofacial hard-tissue defects [in English]. *STEM CELLS TRANSLATIONAL MEDICINE.* 2014;3:530-540.
13. Long T, Zhu Z, Awad HA, Schwarz EM, Hilton MJ, Dong Y. The effect of mesenchymal stem cell sheets on structural allograft healing of critical sized femoral defects in mice. *Biomaterials.* 2014;35(9):2752-2759.
14. Hoffman MD, Xie C, Zhang X, Benoit DSW. The effect of mesenchymal stem cells delivered via hydrogel-based tissue engineered periosteum on bone allograft healing. *Biomaterials.* 2013;34(35):8887-8898.
15. Cornejo A, Sahar DE, Stephenson SM, et al. Effect of adipose tissue-derived osteogenic and endothelial cells on bone allograft osteogenesis and vascularization in critical-sized calvarial defects. *Tissue Eng Part A.* 2012;18(15-16):1552-1561.
16. Zuk PA, Zhu M, Ashjian P, et al. Human adipose tissue is a source of multipotent stem cells. *Mol Biol Cell.* 2002;13(12):4279-4295.
17. Bianco P, Riminucci M, Gronthos S, Robey PG. Bone marrow stromal stem cells: nature, biology, and potential applications [in English]. *STEM CELLS.* 2001;19(3):180-192.
18. Krampera M, Pizzolo G, Aprili G, Franchini M. Mesenchymal stem cells for bone, cartilage, tendon and skeletal muscle repair [in English]. *Bone.* 2006;39(4):678-683.
19. de Girolamo L, Lopa S, Arrigoni E, et al. Human adipose-derived stem cells isolated from young and elderly women: their differentiation potential and scaffold interaction during in vitro osteoblastic differentiation. *Cytotherapy.* 2009;11(6):793-803.
20. Yukata K, Xie C, Li TF, et al. Aging periosteal progenitor cells have reduced regenerative responsiveness to bone injury and to the anabolic actions of PTH 1-34 treatment. *Bone.* 2014;62:79-89.
21. Lavasani M, Robinson AR, Lu A, et al. Muscle-derived stem/progenitor cell dysfunction limits healthspan and lifespan in a murine progeria model. *Nat Commun.* 2012;3:608.
22. Wu T, Chen G, Tian F, Liu HX. Contribution of cranial neural crest cells to mouse skull development. *Int J Dev Biol.* 2017;61(8-9):495-503.
23. Senarath-Yapa K, Li S, Meyer NP, Longaker M, Quarto N. Integration of multiple signaling pathways determines differences in the osteogenic potential and tissue regeneration of neural crest-derived and mesoderm-derived calvarial bones. *Int J Mol Sci.* 2013;14(3):5978-5997.
24. Gitton Y, Heude E, Vieux-Rochas M, et al. Evolving maps in craniofacial development. *Semin Cell Dev Biol.* 2010;21(3):301-308.
25. Jiang X, Gwyne Y, McKeown SJ, et al. Isolation and characterization of neural crest stem cells derived from in vitro-differentiated human embryonic stem cells. *Stem Cells Dev.* 2009;18(7):1059-1070.
26. Liu JA, Cheung M. Neural crest stem cells and their potential therapeutic applications. *Dev Biol.* 2016;419(2):199-216.
27. Menendez L, Kulik MJ, Page AT, et al. Directed differentiation of human pluripotent cells to neural crest stem cells. *Nat Protoc.* 2013;8(1):203-212.
28. Menendez L, Yatskievych TA, Antin PB, Dalton S. Wnt signaling and a Smad pathway blockade direct the differentiation of human pluripotent stem cells to multipotent neural crest cells. *Proc Natl Acad Sci USA.* 2011;108(48):19240-19245.
29. Lee G, Chambers SM, Tomishima MJ, Studer L. Derivation of neural crest cells from human pluripotent stem cells. *Nat Protoc.* 2010;5(4):688-701.
30. Muhammad A, Kim K, Epifantseva I, et al. Cell transplantation strategies for acquired and inherited disorders of peripheral myelin. *Ann Clin Transl Neurol.* 2018;5(2):186-200.
31. Sheyn D, Shapiro G, Tawackoli W, et al. PTH induces systemically administered mesenchymal stem cells to migrate to and regenerate spine injuries. *Mol Ther.* 2016;24(2):318-330.
32. Sheyn D, Cohn-Yakubovich D, Ben-David S, et al. Bone-chip system to monitor osteogenic differentiation using optical imaging [in English]. *Microfluid Nanofluidics.* 2019;23(99):1-10.
33. Sheyn D, Kallai I, Tawackoli W, et al. Gene-modified adult stem cells regenerate vertebral bone defect in a rat model. *Mol Pharm.* 2011;8(5):1592-1601.
34. Kimelman NB, Kallai I, Sheyn D, et al. Real-time bioluminescence functional imaging for monitoring tissue formation and regeneration. *Methods Mol Biol.* 2013;1048:181-193.
35. Cohn Yakubovich D, Eliav U, Yalon E, et al. Teriparatide attenuates scarring around murine cranial bone allograft via modulation of angiogenesis. *Bone.* 2017;97:192-200.
36. Sheyn D, Cohn Yakubovich D, Kallai I, et al. PTH promotes allograft integration in a calvarial bone defect. *Mol Pharm.* 2013;10(12):4462-4471.
37. Sheyn D, Ben-David S, Tawackoli W, et al. Human iPSCs can be differentiated into notochordal cells that reduce intervertebral disc degeneration in a porcine model. *Theranostics.* 2019;9(25):7506-7524.
38. Sheyn D, Ben-David S, Shapiro G, et al. Human iPSCs differentiate into functional MSCs and repair bone defects. *STEM CELLS TRANSLATIONAL MEDICINE.* 2016;5:1447-1460.
39. Sheyn D, Pelled G, Netanel D, Domany E, Gazit D. The effect of simulated microgravity on human mesenchymal stem cells cultured in an osteogenic differentiation system: a bioinformatics study. *Tissue Eng Part A.* 2010;16(11):3403-3412.
40. Aslan H, Zilberman Y, Arbeli V, et al. Nucleofection-based ex vivo nonviral gene delivery to human stem cells as a platform for tissue regeneration. *Tissue Eng.* 2006;12(4):877-889.
41. Aslan H, Zilberman Y, Kandel L, et al. Osteogenic differentiation of noncultured immunoisolated bone marrow-derived CD105+ cells. *STEM CELLS.* 2006;24(7):1728-1737.
42. Mizrahi O, Sheyn D, Tawackoli W, et al. BMP-6 is more efficient in bone formation than BMP-2 when overexpressed in mesenchymal stem cells. *Gene Ther.* 2013;20(4):370-377.
43. Sheyn D, Ben-David S, Shapiro G, et al. Human induced pluripotent stem cells differentiate into functional mesenchymal stem cells and repair bone defects. *STEM CELLS TRANSLATIONAL MEDICINE.* 2016;5(11):1447-1460.
44. Dominici M, Le Blanc K, Mueller I, et al. Minimal criteria for defining multipotent mesenchymal stromal cells. The International Society for Cellular Therapy position statement [in English]. *Cytotherapy.* 2006;8(4):315-317.
45. Sheyn D, Pelled G, Tawackoli W, et al. Transient overexpression of Ppargamma2 and C/ebpalpha in mesenchymal stem cells induces brown adipose tissue formation. *Regen Med.* 2013;8(3):295-308.
46. Kuroda T, Yasuda S, Kusakawa S, et al. Highly sensitive in vitro methods for detection of residual undifferentiated cells in retinal pigment epithelial cells derived from human iPSC cells. *PLoS One.* 2012;7(5):e37342.
47. Pennington EC, Dionigi B, Gray FL, et al. Limb reconstruction with decellularized, non-demineralized bone in a young leporine model. *Biomed Mater.* 2015;10(1):015021.
48. Hung BP, Salter EK, Temple J, et al. Engineering bone grafts with enhanced bone marrow and native scaffolds. *Cells Tissues Organs.* 2013;198(2):87-98.
49. Gupta DM, Kwan MD, Slater BJ, Wan DC, Longaker MT. Applications of an athymic nude mouse model of nonhealing critical-sized calvarial defects. *J Craniofac Surg.* 2008;19(1):192-197.
50. Cowan CM, Aghaloo T, Chou YF, et al. MicroCT evaluation of three-dimensional mineralization in response to BMP-2 doses in vitro and in critical sized rat calvarial defects. *Tissue Eng.* 2007;13(3):501-512.

51. Jin Q, Giannobile WV. SDF-1 enhances wound healing of critical-sized calvarial defects beyond self-repair capacity. *PLoS One*. 2014;9(5):e97035.
52. Kimelman-Bleich N, Pelled G, Zilberman Y, et al. Targeted gene-and-host progenitor cell therapy for nonunion bone fracture repair [in English]. *Mol Ther*. 2011;19(1):53-59.
53. Kallai I, Mizrahi O, Tawackoli W, Gazit Z, Pelled G, Gazit D. Micro-computed tomography-based structural analysis of various bone tissue regeneration models [in English]. *Nat Protoc*. 2011;6(1):105-110.
54. Sheyn D, Kallai I, Tawackoli W, et al. Gene-modified adult stem cells regenerate vertebral bone defect in a rat model [in English]. *Mol Pharm*. 2011;8(5):1592-1601.
55. Reynolds DG, Shaikh S, Papuga MO, et al. muCT-based measurement of cortical bone graft-to-host union. *J Bone Miner Res*. 2009;24(5):899-907.
56. Yeo A, Wong WJ, Teoh SH. Surface modification of PCL-TCP scaffolds in rabbit calvaria defects: evaluation of scaffold degradation profile, biomechanical properties and bone healing patterns. *J Biomed Mater Res A*. 2010;93(4):1358-1367.
57. Diao J, OuYang J, Deng T, et al. 3D-plotted beta-tricalcium phosphate scaffolds with smaller pore sizes improve in vivo bone regeneration and biomechanical properties in a critical-sized calvarial defect rat model. *Adv Healthc Mater*. 2018;7(17):e1800441.
58. Lohmann P, Willuweit A, Neffe AT, et al. Bone regeneration induced by a 3D architected hydrogel in a rat critical-size calvarial defect. *Biomaterials*. 2017;113:158-169.
59. Sheyn D, Kimelman-Bleich N, Pelled G, Zilberman Y, Gazit D, Gazit Z. Ultrasound-based nonviral gene delivery induces bone formation in vivo. *Gene Ther*. 2008;15(4):257-266.
60. Pittenger MF, Mackay AM, Beck SC, et al. Multilineage potential of adult human mesenchymal stem cells. *Science*. 1999;284(5411):143-147.
61. Horibata S, Vo TV, Subramanian V, et al. Utilization of the soft agar colony formation assay to identify inhibitors of tumorigenicity in breast cancer cells. *J Vis Exp*. 2015;(99):e52727.
62. Walmsley GG, Senarath-Yapa K, Wearda TL, et al. Surveillance of stem cell fate and function: a system for assessing cell survival and collagen expression in situ. *Tissue Eng Part A*. 2016;22(1-2):31-40.
63. Wang S, Zhao Z, Yang Y, et al. A high-strength mineralized collagen bone scaffold for large-sized cranial bone defect repair in sheep. *Regen Biomater*. 2018;5(5):283-292.
64. Al-Hezaimi K, Ramalingam S, Al-Askar M, et al. Real-time-guided bone regeneration around standardized critical size calvarial defects using bone marrow-derived mesenchymal stem cells and collagen membrane with and without using tricalcium phosphate: an in vivo micro-computed tomographic and histologic experiment in rats. *Int J Oral Sci*. 2016;8(1):7-15.
65. Adamzyk C, Kachel P, Hoss M, et al. Bone tissue engineering using polyetherketoneketone scaffolds combined with autologous mesenchymal stem cells in a sheep calvarial defect model. *J Craniomaxillofac Surg*. 2016;44(8):985-994.
66. Chen P, Miller PD, Recker R, et al. Increases in BMD correlate with improvements in bone microarchitecture with teriparatide treatment in postmenopausal women with osteoporosis. *J Bone Miner Res*. 2007;22(8):1173-1180.
67. Stenstrom M, Olander B, Lehto-Axtelius D, et al. Bone mineral density and bone structure parameters as predictors of bone strength: an analysis using computerized microtomography and gastrectomy-induced osteopenia in the rat. *J Biomech*. 2000;33(3):289-297.
68. Bouxsein ML, Boyd SK, Christiansen BA, Guldborg RE, Jepsen KJ, Müller R. Guidelines for assessment of bone microstructure in rodents using micro-computed tomography. *J Bone Miner Res*. 2010;25(7):1468-1486.
69. Li X, Zhang R, Tan X, Li B, Liu Y, Wang X. Synthesis and evaluation of BMMSC-seeded BMP-6/nHAG/GMS scaffolds for bone regeneration. *Int J Med Sci*. 2019;16(7):1007-1017.
70. James AW, LaChaud G, Shen J, et al. A review of the clinical side effects of bone morphogenetic protein-2. *Tissue Eng Part B Rev*. 2016;22(4):284-297.
71. Suenaga H, Furukawa KS, Suzuki Y, Takato T, Ushida T. Bone regeneration in calvarial defects in a rat model by implantation of human bone marrow-derived mesenchymal stromal cell spheroids. *J Mater Sci Mater Med*. 2015;26(11):254.

SUPPORTING INFORMATION

Additional supporting information may be found online in the Supporting Information section at the end of this article.

How to cite this article: Glaeser JD, Behrens P, Stefanovic T, et al. Neural crest-derived mesenchymal progenitor cells enhance cranial allograft integration. *STEM CELLS Transl Med*. 2021;10:797-809. <https://doi.org/10.1002/sctm.20-0364>